

Preparation of F-Doped TiO₂ Photocatalysts by Gas–Liquid Plasma at Atmospheric Pressure

Xiuling Zhang¹ · Zhuang Li¹ · Zhibin Zhan¹ · Lanbo Di¹

Published online: 10 April 2017
© Springer Science+Business Media New York 2017

Abstract F-Doped TiO₂ was successfully fabricated using gas–liquid cold plasma with different fluorine sources, including NaF, NaF combined with [C₄MIM]HSO₄, and [C₄MIM]BF₄. The samples were characterized by XRD (X-ray diffraction), XPS (X-ray photoelectron spectroscopy), and BET (N₂ adsorption–desorption isotherms). Photocatalytic activity of the samples was tested by degradation of methylene blue (MB) dye under simulated sunlight. The results show that doping with different fluorine sources was beneficial to form interstitial F-doped TiO₂, and ionic liquids used in our work were most favorable to the formation of interstitial F-doped TiO₂. Calcination of the 0.6-F–[C₄MIM]BF₄–TiO₂ sample at 500 °C shows that interstitial F-doped TiO₂ has an excellent thermal stability, a suitable mesoporous structure, higher specific surface area (60.5 m² g⁻¹) and the best photocatalytic activity. MB degradation was about 98% under the stimulated sunlight for 30 min, and its apparent rate constant was 42 times higher than photolysis and was about 2.9 times as that prepared without addition of ionic liquid. Furthermore, the stability of ionic liquids in the gas–liquid plasma was also investigated and discussed with the assistance of Fourier transform infrared (FTIR) spectroscopy.

Keywords Gas–liquid plasma · Dielectric barrier discharge · F-Doped · TiO₂ · Ionic liquid

1 Introduction

Titanium dioxide (TiO₂) is the most promising photocatalyst and has drawn much research attentions due to its high efficiency, low cost, non-toxicity and high photo-stability [1–5]. However, the application of TiO₂ has been limited owing to its large band gap energy (3.20 eV for anatase TiO₂), which is not helpful to fully use of the sunlight. Doping with non-metal ions such as N, C, B and F has been proved to be an efficient method to narrow the band gap of TiO₂ and to broader light response range towards visible wavelength [6–9]. Among these non-metal elements, doping TiO₂ with F has been demonstrated an effective approach to enhance its visible light photocatalytic activity. Yu et al. [10] synthesized F-doped TiO₂ with NH₄F and tetrabutyl titanate using a modified sol–gel method including a process of drying in air at 100 °C for 24 h and then heating at 500 °C. The F-doped TiO₂ exhibited an enhanced photocatalytic performance for MB degradation with a degradation rate of 91% compared to pure TiO₂ (32%). Pan et al. [11] prepared mesoporous F–TiO₂ spheres consisting of anatase nanocrystallites using titanium alkoxides and NH₄F as Ti and F precursors, respectively. After calcination at 450 °C for 2 h, the obtained mesoporous F–TiO₂ spheres showed superior photocatalytic activity in dye degradation. These traditional sol–gel or solvothermal methods indicated that synthesizing F-doped TiO₂ is a good strategy to improve the photocatalytic performance of TiO₂.

Recently, gas–liquid plasma technology has been developed and has been used to treat waste water, promote chemical reactions and prepare nanomaterials

Electronic supplementary material The online version of this article (doi:10.1007/s11244-017-0763-7) contains supplementary material, which is available to authorized users.

✉ Xiuling Zhang
xiulz@sina.com

✉ Lanbo Di
dilanbo@163.com

¹ College of Physical Science and Technology, Dalian University, Dalian 116622, China

[12–15]. Ionic liquids (ILs), which consists of only positive and negative ions, have extremely low vapor pressure, high heat capacity and chemical stability. They have been successfully used in different kinds of reactions as green reaction media. The interaction of plasma and ionic liquid may change the properties of plasma and thus vary the intensity and direction of the gaseous phase reaction in the plasma. Yu et al. [13] reported the catalytic action of nine imidazolium-based ionic liquids for methane conversion in a direct current (DC) discharge plasma. Ionic liquid $C_6MIMHSO_4$ (1-hexyl-3-methylimidazolium hydrogen sulphate) enhanced the conversion of methane and C_6MIMBF_4 (1-hexyl-3-methylimidazolium tetrafluoroborate) increased the selectivity of C_2 hydrocarbons. Zhou et al. [16] investigated SiO_2 supported ionic liquid with Pd systems for the selective hydrogenation of acetylene with the assistance of RF non-thermal plasma. The results suggested that supported Pd catalysts loaded with ionic liquids were effective for selective hydrogenation of acetylene in ethylene. The catalysts with ionic liquids of BF_4^- anions usually achieve higher conversion but lower selectivity, and those catalysts with PF_6^- anions give lower conversion but higher selectivity. Zhang et al. [17] studied the influences of $\gamma-Al_2O_3$ supported C_6MIMBF_4 and Pd on methane conversion to C_2 hydrocarbons under cold plasma. The results indicated that the selectivity and yield of C_2 hydrocarbons were increased with the increase in immobilization amount of C_6MIMBF_4 . Furthermore, plasma also enhances the synthetic reaction in the ionic liquid or water and ionic liquid mixed solution. Wei et al. [18] gained gold nanoparticles using the subatmospheric dielectric barrier discharge plasma reduction in the C_4MIMBF_4 (1-butyl-3-methylimidazolium tetrafluoroborate). Hatakeyama et al. [14] presented an effective preparation method of Au nanoparticles (NPs) in an arc plasma deposition technique combined with ionic liquids as capture media. Tran et al. [15] synthesized Platinum nanoparticles (PtNPs) using a liquid plasma system with C_4MIMBF_4 under atmospheric pressure. Zhang et al. [19] prepared anatase–rutile mixed phase TiO_2 with high photocatalytic activity by atmospheric-pressure dielectric barrier discharge (DBD) gas–liquid cold plasma using C_4MIMBF_4 as assistant.

In this work, F-doped anatase TiO_2 photocatalysts were synthesized by atmospheric-pressure gas–liquid cold plasma, using titanium oxysulfate as Ti precursor and NaF solution, mixed solution of NaF and $[C_4MIM]HSO_4$, and $[C_4MIM]BF_4$ as the F precursor. The phase structure, doping type, thermal stability and photocatalytic performance of the F-doped TiO_2 samples have been investigated.

2 Experimental

2.1 Materials

Titanium oxysulfate [$TiOSO_4$, analytical reagent (AR)-grade] was obtained from Tianjin Guangfu Fine Chemical Research Institute, China. Sodium fluoride [NaF, analytical reagent (AR)-grade] was obtained from Aladdin. 1-Butyl-3-methylimidazolium tetrafluoroborate ($[C_4MIM]BF_4$ ionic liquid, purity >99%) and 1-butyl-3-methylimidazolium hydrogen sulphate ($[C_4MIM]HSO_4$ ionic liquid, purity >99%) were purchased from Lanzhou Institute of Chemical Physics, Chinese Academy of Sciences, China. All of the materials were used as received.

2.2 Catalyst Preparation

The preparation process was similar with our previous work [19]. Briefly, certain amount of fluorine sources (0.8 g NaF, the mixture of 0.8 g NaF and 0.6 mL $[C_4MIM]HSO_4$, or 0.6 mL $[C_4MIM]BF_4$) were added to the solution of 10 g $TiOSO_4$ and 50 mL deionized water under vigorous stirring to obtain the mixture of Ti precursors solution containing the fluorine source. Then the process of plasma treatment was conducted to prepare the fluoride-doped TiO_2 (F– TiO_2) photocatalysts, which was performed at atmospheric pressure in open air for twice, with an interval of 5 min between the two operations. Each treatment just takes 5 min. Then the obtained solution was filtered, washed and dried under vacuum for 2 h at 100 °C to remove the impurities remaining in the TiO_2 networks. Corresponding to the different fluorine sources (NaF, NaF combined with $[C_4MIM]HSO_4$, and $[C_4MIM]BF_4$), the obtained samples are denoted as F– TiO_2 , F– $[C_4MIM]HSO_4$ – TiO_2 and F– $[C_4MIM]BF_4$ – TiO_2 , respectively.

The schematic diagram of the atmospheric-pressure DBD gas–liquid cold plasma device for preparing F-doped TiO_2 photocatalysts can be seen in previous work [20]. A quartz reaction cell (60 mm in diameter) was placed between the high-voltage electrode and ground electrode, both of which were made of stainless steel (50 mm in diameter). The two quartz dielectrics were both 1 mm thick, and the discharge gap was 4 mm. A sinusoidal high voltage at a frequency of 14.2 kHz was applied to conduct the plasma treatment with a CTP-2000K power source provided by Nanjing Suman Electronic Co. Ltd, China.

2.3 Catalyst Characterization

The F-doped TiO_2 samples were characterized by powder X-ray diffraction (XRD) on an X-ray diffractometer (DX-2700, Dandong Haoyuan, China) using Cu $K\alpha 1$ radiation ($\lambda = 1.54178 \text{ \AA}$) with a step-scan of 0.03 degree per step,

corresponding to 3.6 degree per minute. The chemical compositions of the samples were investigated by X-ray photoelectron spectroscopy (XPS, ESCALAN250 Thermo VG) using a monochromatized AlK α (1486.6 eV) X-ray source. All binding energies were referenced to the XPS peak of carbon 1 s at 284.6 eV. The pore size (D_p) distributions, Brunauer–Emmett–Teller (BET) surface areas (S_{BET}), and pore volumes (V_p) were measured by nitrogen adsorption and desorption using a gas sorption analyzer (NOVA 2200e, Quantachrome Corp., USA). Prior to the adsorption analysis, the samples were outgassed at 200 °C for 5 h in the degassing port of the analyzer. The C₄MIMBF₄ used before and after gas–liquid plasma treatment was detected on a Spectrum one-B FTIR (PerkinElmer).

2.4 Photocatalytic Activity Test

Photocatalytic activity of the F–TiO₂ samples was tested based on the degradation of a methylene blue (MB) dye solution using a 300 W Xe lamp. Detailed information about the photocatalytic activity test can be found in our previous work [21]. In brief, the photocatalytic reaction was carried out with 0.1 g catalyst suspended in 100 mL of a MB solution (10 mg L⁻¹) in a Pyrex glass cell. The solution, which was kept at pH=6, was stirred in the dark for 30 min to obtain a good dispersion and established the adsorption–desorption equilibrium between the MB molecules and the catalyst surface. At given time intervals, the slurry samples including the photocatalysts and MB were centrifuged and the solution was analyzed with a UV–visible spectrometer (721 Spectrophotometer, Shanghai Jinghua Group Co., Ltd, China). Since good linear relationship between the concentration and the absorption of MB was obtained at the wavelength of 665 nm, the MB degradation η is defined as

$$\eta = \frac{c_0 - c}{c_0} \times 100\% \quad (1)$$

where c_0 is the initial concentration of MB (mg L⁻¹) and c is the concentration of MB (mg L⁻¹) at a certain time.

3 Results and Discussion

3.1 Effect of Fluorine Sources on the Phase Structure of TiO₂

Figure 1 shows the XRD patterns of TiO₂ and F-doped TiO₂ samples prepared with different fluorine sources (NaF, NaF combined with [C₄MIM]HSO₄, and [C₄MIM]BF₄), namely F–TiO₂, F–[C₄MIM]HSO₄–TiO₂ and F–[C₄MIM]BF₄–TiO₂ samples. As shown in Fig. 1, the diffraction peaks at 25.3° and 48.0° appeared, which were indexed

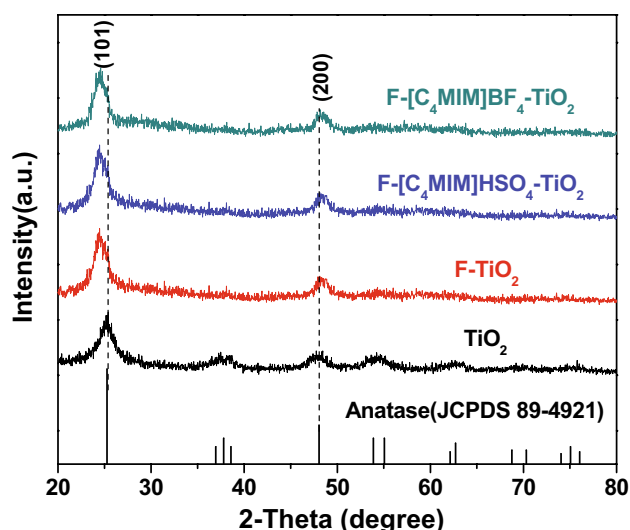


Fig. 1 XRD patterns of F-doped TiO₂ prepared by gas–liquid plasma with different fluorine sources

to (101) and (200) reflections of anatase TiO₂ (PDF No. 21-1272). By carefully comparing the diffraction peaks for (101) and (200) in the three F-doped TiO₂, we can find that the (101) diffraction peaks at round 25° shift to lower 2θ values, while the (200) diffraction peaks at around 48.0° shift toward higher 2θ values. Similar phenomenon was also observed in the work when doping with fluorine in preparing ZnWO₄ catalyst [22, 23]. The shift of the diffraction peak for F-doped TiO₂ samples indicates that lattice imperfection was formed due to F doping. The fluorine atoms enter into the lattice of TiO₂, therefore breaks the equilibrium of original TiO₂ atoms and varies the interplanar crystal spacing of anatase TiO₂. The Bragg equation illustrated below clearly reveals the functional relationship between the interplanar crystal spacing and the diffraction angle:

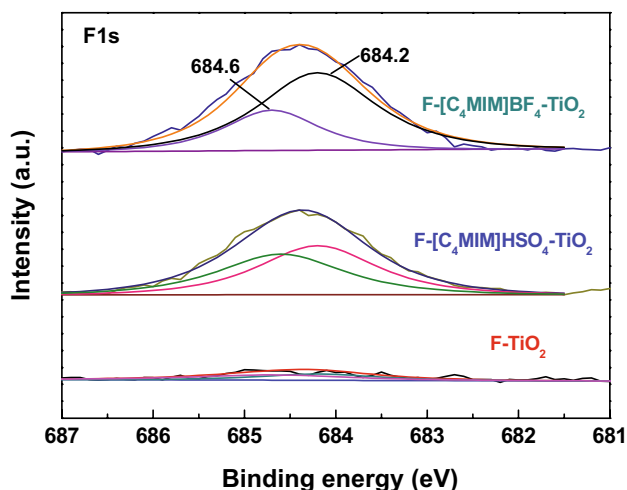
$$d_{(hkl)} = \frac{n\lambda}{2 \sin \theta} \quad (2)$$

where $d_{(hkl)}$ is the interplanar crystal spacing, λ is the wavelength of X ray and θ is the angle between X ray and the (hkl) crystal face. When doping with fluorine, the $d_{(hkl)}$ value is varied by the lattice deformation and the value of θ changes correspondingly, and the change of θ value becomes greater when the dopants of fluorine increases.

Table 1 demonstrates the relative shift values of diffraction angle at around 25.3° and 48.0° of F-doped TiO₂ prepared with different fluorine sources. The relative shift value of diffraction angle for the diffraction peak at around 25.3° for F–TiO₂ samples is 0.8°, while the relative shift value for the diffraction peak at around 48.0° is 0.2°. As for the F–[C₄MIM]HSO₄–TiO₂ and F–[C₄MIM]BF₄–TiO₂

Table 1 Angular deviation of XRD diffraction peak at 25.3° and 48.0° of F-doped TiO₂ prepared with different fluorine sources

| Samples | 2θ | Relative shift (toward lower 2θ value) | 2θ | Relative shift (toward higher 2θ value) |
|--|-------|--|-------|---|
| Anatase TiO ₂ | 25.3° | – | 48.0° | – |
| F–TiO ₂ | 24.5° | 0.8° | 48.2° | 0.2° |
| F–[C ₄ MIM]HSO ₄ –TiO ₂ | 24.3° | 1.0° | 48.4° | 0.4° |
| F–[C ₄ MIM]BF ₄ –TiO ₂ | 24.3° | 1.0° | 48.4° | 0.4° |

**Fig. 2** XPS spectra of F1s in F–TiO₂, F–[C₄MIM]HSO₄–TiO₂ and F–[C₄MIM]BF₄–TiO₂

samples, the shift values are both 1.0° for the diffraction peak at around 25.3° and 0.4° for the diffraction peak at around 48.4°, which are greater than the F–TiO₂ samples. This reveals that [C₄MIM]HSO₄ and [C₄MIM]BF₄ used here are helpful for the formation of F-doped TiO₂.

3.2 Effect of Fluorine Sources on the F Doping Types of TiO₂

The XPS spectra of F1s in F–TiO₂, F–[C₄MIM]HSO₄–TiO₂ and F–[C₄MIM]BF₄–TiO₂ samples are shown in Fig. 2. The F1s peaks were observed in all of the F-doped TiO₂ samples, and may be divided into two peaks at 684.2 and 684.6 eV with Gaussian distributions. Specifically, the peak at 684.2 eV is assigned to the F[–] ions that are physically adsorbed on the surface of TiO₂ [23–25]. According to the literature [24, 25], the peak at around 688.7 eV is the F in solid solution TiO_{2–x}F_x formed by the substitution of O^{2–} with F[–]. Therefore the peak at 684.6 eV observed here should be ascribed to the interstitial doping F[–] ions in TiO₂ lattice. As we know, the structure of anatase TiO₂ belongs to the tetragonal system, which is composed of TiO₆ octahedron. The O^{2–} ions in TiO₂ are closely packed to form octahedral interstices and tetrahedral interstices. Half of

the octahedral interstices may be occupied by the Ti⁴⁺ ions to form TiO₆ octahedron, while the left octahedral interstices and tetrahedral interstices are vacant. There are two methods for preparing F-doped TiO₂. One is substitution of F[–] for O^{2–} in the TiO₂ lattice crystal. Since the atomic radii of F[–] (0.133 nm) and O^{2–} (0.140 nm) are about the same, the substitutional F-doping will not change the lattice spacing of TiO₂. Therefore, as confirmed by the XRD test and the Bragg equation discussed above, the observed shift of diffraction peak toward lower angle may not be due to the smaller lattice parameter resulted from the substitution of O^{2–} by F[–] [24–28]. The other kind of F-doping is interstitial doping. Since the atomic radius of F[–] is large, it can only enter into the octahedral void with large space, and a small change in lattice parameter may occur. This may result in the change of lattice space and the shift of diffraction peak [22, 23].

Furthermore, the F1s peak areas of the three F-doped TiO₂ samples are significantly different. The peak area of interstitial doping F[–] ions for F–TiO₂ is much smaller than the F–[C₄MIM]HSO₄–TiO₂ and F–[C₄MIM]BF₄–TiO₂ samples. In conclusion, all of the F-doped TiO₂ samples prepared with gas–liquid plasma present the interstitial F doping, and the ionic liquids of [C₄MIM]HSO₄ and [C₄MIM]BF₄ are beneficial to the entrance of F[–] ions into the interstitial space of TiO₂ lattice.

3.3 Thermal Stability of the F-Doped TiO₂

In order to investigate the thermal stability of the F-doped TiO₂ samples, F–TiO₂, F–[C₄MIM]HSO₄–TiO₂ and F–[C₄MIM]BF₄–TiO₂ were calcined at 500 °C for 2 h, and denoted as F–TiO₂-500 °C, F–[C₄MIM]HSO₄-TiO₂-500 °C and F–[C₄MIM]BF₄-TiO₂-500 °C, respectively. XRD patterns of the F-doped TiO₂ samples are shown in Fig. 3. It demonstrates that after calcination the diffraction peak at around 25.3° has no shift for the F–TiO₂-500 °C sample, however, it still shifts to a lower diffraction angle for F–[C₄MIM]HSO₄-TiO₂-500 °C and F–[C₄MIM]BF₄-TiO₂-500 °C. It reveals that the interstitially doped fluorine impurities within F–TiO₂-500 °C are not as thermally stable as the other two samples. Besides, the shift of diffraction peaks of F–[C₄MIM]HSO₄-TiO₂-500 °C and F–[C₄MIM]

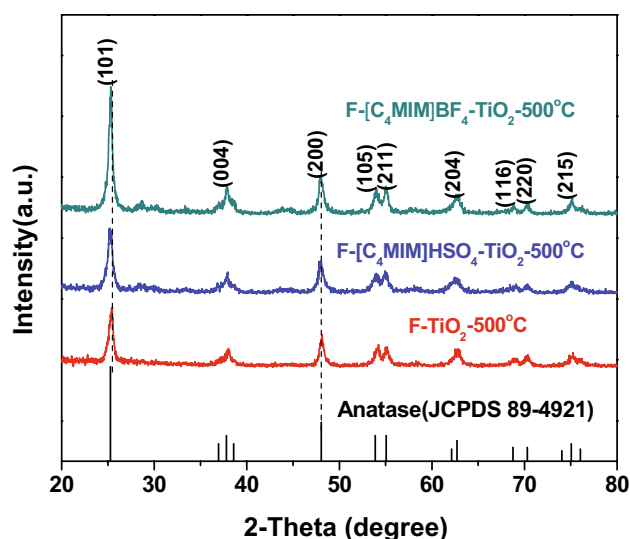


Fig. 3 XRD patterns of F-doped TiO₂ with different fluorine sources calcined at 500 °C

BF₄-TiO₂-500 °C sample is smaller (from 1.0° decreasing to 0.4°) after calcination, indicating the decrease of interstitial doping F contents in these two samples. Furthermore, all of the diffraction peaks of samples after calcination show a higher intensity, which shows that the calcination process may enhance the crystallization of F-doped TiO₂. Interestingly, the diffraction peaks of the TiO₂ samples are greater enhanced when using ionic liquids as the fluorine sources. Thus it may be concluded that the fluorine sources have significant effect both on the thermal stability and crystallinity of the F-doped TiO₂ samples.

XPS spectra of F1s in F-doped TiO₂ with different fluorine sources calcined at 500 °C were also obtained, as shown in Fig. 4. As for F-TiO₂-500 °C, the physically adsorbed and interstitial doping F⁻ ions at around 684 eV disappeared. For F-[C₄MIM]HSO₄-TiO₂-500 °C and F-[C₄MIM]BF₄-TiO₂-500 °C, only the interstitial doping F⁻ ions at the binding energy of 684.6 eV were observed, and the intensities were decreased compared with the samples without calcination. Vanish of the physically adsorbed F⁻ ions for F-doped TiO₂ samples indicated that calcination played an important role on the stability of F-doped TiO₂, and ionic liquid is beneficial to enhance the stability of interstitial F-doping TiO₂.

The N₂ absorption-desorption isotherms and pore size distributions of F-doped TiO₂ samples with different fluorine sources calcined at 500 °C are also observed and illustrated in Fig. 5 and Table 2. All of the calcined F-doped TiO₂ samples exhibit type-IV isotherm plots and H3 hysteresis loop [20], as shown in Fig. 5a. In addition, there is no significant difference between their specific surface area, which indicates that the pore structure of F-doped

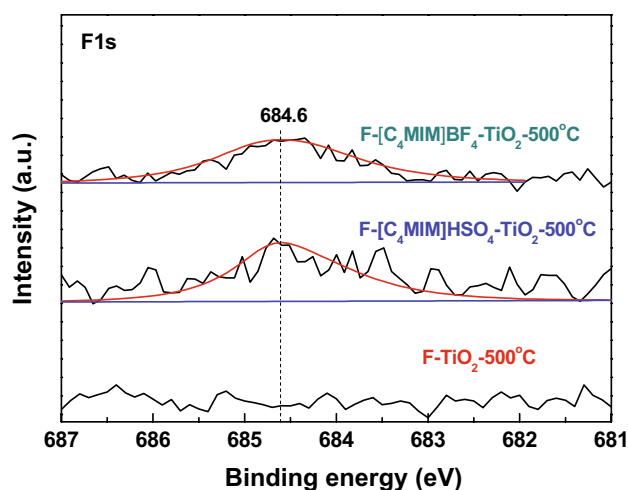


Fig. 4 XPS spectra of F1s in F-doped TiO₂ with different fluorine sources calcined at 500 °C

TiO₂ samples is thermally stable against the calcination at 500 °C.

3.4 Photocatalytic Activity of the Post-Calcined F-Doped TiO₂

Figure 6a represents the MB photodegradation over F-TiO₂-500 °C, F-[C₄MIM]HSO₄-TiO₂-500 °C and F-[C₄MIM]BF₄-TiO₂-500 °C under simulated sunlight. It has been shown that the F-doped TiO₂ photocatalysts prepared by gas-liquid plasma using different fluorine sources and calcined at 500 °C all showed high photocatalytic activity for MB degradation. The F-[C₄MIM]BF₄-TiO₂ shows the best activity for MB photodegradation. According to the values taken from Fig. 6a, ln(*c*₀/*c*) for the samples was plotted against the irradiation time, as shown in Fig. 6b. Good linear relationships between the two parameters were obtained, which confirms the pseudo-first-order reaction for the degradation of MB as discussed in previous work [19].

The apparent rate constants (*k*) of MB photodegradation, obtained from the slopes of the best-fit lines, are 0.0252, 0.0390 and 0.0719 min⁻¹, for F-TiO₂-500 °C, F-[C₄MIM]HSO₄-TiO₂-500 °C and F-[C₄MIM]BF₄-TiO₂-500 °C, respectively (Fig. 6c). The apparent rate constant for MB photodegradation over F-[C₄MIM]BF₄-TiO₂-500 °C is the highest and is 42 times higher than photolysis (0.0017 min⁻¹), and was about 2.9 times as that prepared without addition of ionic liquid.

3.5 The Stability of ILs in Preparing F-Doped TiO₂ by Gas-Liquid Plasma

The process of preparing F-doped TiO₂ by gas-liquid plasma is a fast reaction. During the preparation process,

Fig. 5 **a** N_2 absorption–desorption isotherms and **b** pore size distributions of F-doped TiO_2 samples with different fluorine sources calcined at $500^\circ C$

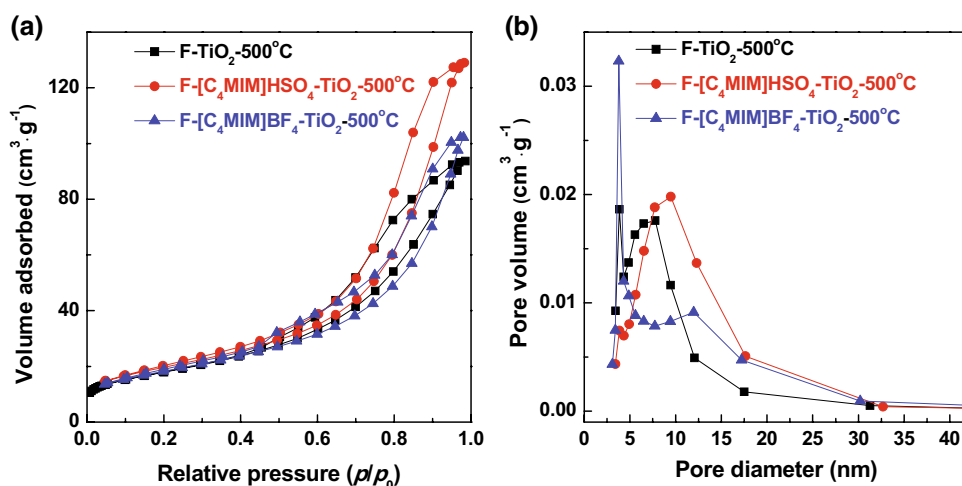


Table 2 Pore volume (V_p), pore diameter (D_p) and specific surface area (S_{BET}) of F-doped TiO_2 prepared with different fluorine sources calcined at $500^\circ C$

| Samples | $V_p/(cm^3 g^{-1})$ | $D_p/(nm)$ | $S_{BET}/(m^2 g^{-1})$ |
|--|---------------------|------------|------------------------|
| F- TiO_2 - $500^\circ C$ | 0.02 | 7.21 | 64.1 |
| F- $[C_4MIM]HSO_4$ - TiO_2 - $500^\circ C$ | 0.02 | 9.47 | 68.1 |
| F- $[C_4MIM]BF_4$ - TiO_2 - $500^\circ C$ | 0.03 | 3.79 | 65.0 |

part of the F^- ions are physically absorbed on the surface of TiO_6 precursors, while others enter into the tetrahedral interstices formed by O^{2-} ions, which results in interstitial doping F^- ions. As discussed above, the doped F^- ions are provided by NaF for F- TiO_2 and F- $[C_4MIM]HSO_4$ - TiO_2 samples. However, as for F- $[C_4MIM]BF_4$ - TiO_2 sample, they may be derived from the decomposition of $[C_4MIM]BF_4$ ionic liquid. Therefore it would be necessary to investigate the stability of $[C_4MIM]BF_4$ ionic liquid during the gas–liquid plasma process.

The FTIR spectra of the C_4MIMBF_4 before (Fig. 7a) and after (Fig. 7b) gas–liquid plasma treatment are showed in Fig. 7. The spectra contains imidazole C–H stretching peaks at 3160 and 2121 cm^{-1} ; an aliphatic C–H stretching at 2958 , 2933 , and 2862 cm^{-1} ; an imidazole C–N stretching at 1574 cm^{-1} ; a methylene C–H scissoring at 1467 cm^{-1} . The peaks at 1170 and 1062 cm^{-1} contribute to the aromatic C–H in-plane bending vibration and B–F stretching, respectively [13]. There is no much difference between the spectra of C_4MIMBF_4 before and after gas–liquid plasma treatment. This indicated that $[C_4MIM]BF_4$ ionic liquid in plasma is stable. This has also been observed for ionic liquid $[C_4MIM]HSO_4$ (Fig. S1).

Furthermore, the amount of F dopants is different for F- TiO_2 , F- $[C_4MIM]HSO_4$ - TiO_2 and F- $[C_4MIM]BF_4$ - TiO_2 samples, as revealed by Figs. 1 and

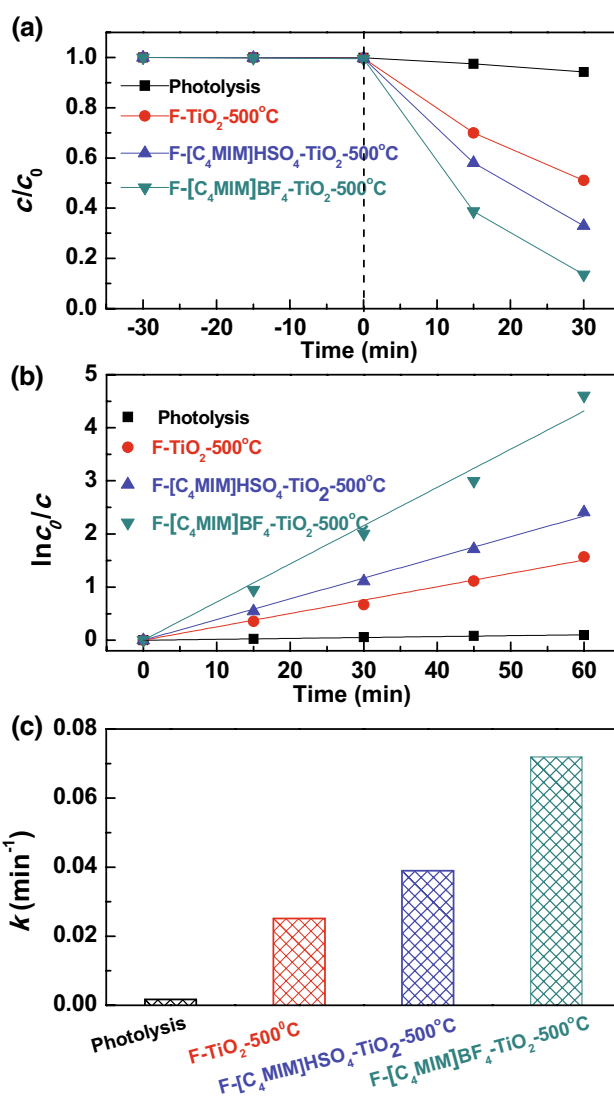


Fig. 6 Photocatalytic activity of F-doped TiO_2 with different fluorine sources calcined at $500^\circ C$ **a** MB photodegradation, **b** $\ln(c_0/c)$ as a function of time and **c** the apparent rate constants (k)

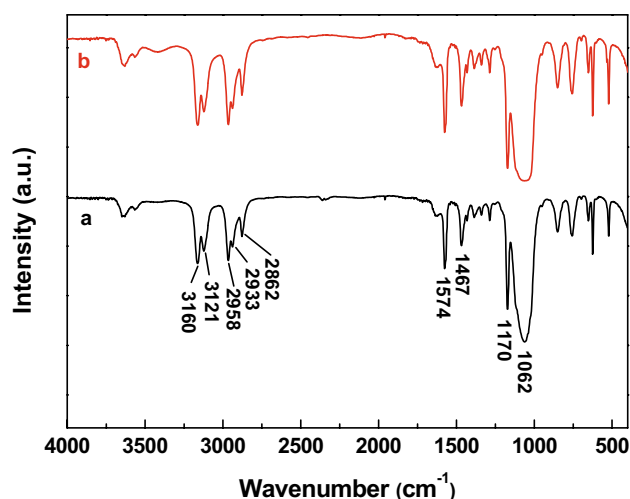


Fig. 7 FTIR spectra of the C_4MIMBF_4 ionic liquid *a* before and *b* after gas–liquid plasma treatment

2. The interstitial F dopants in $F-[C_4MIM]HSO_4-TiO_2$ and $F-[C_4MIM]BF_4-TiO_2$ are relatively higher, which indicates that ionic liquids are helpful for forming interstitial F dopants. This may be explained by the formation of the $\pi-\pi$ bond between imidazole cationic, and the strong hydrogen bond between TiO_6 octahedral and HSO_4 and BF_4 anionic. The $\pi-\pi$ bond, hydrogen bond and Coulomb force could be structure-oriented in the formation of TiO_2 , therefore F^- ions are easier in entering the tetrahedron intervals formed by O^{2-} ions and forming interstitial dopants. Besides, F-doped TiO_2 would nucleate faster in ionic liquids since its interfacial tension is lower. In conclusion, ionic liquids combined with plasma promote the formation of F-doped TiO_2 , proper amount of ionic liquids is conducive for preparing highly photocatalytic activity F-doped TiO_2 . Further work will be conducted to investigate the influence of F doping amounts and discharge parameters.

4 Conclusion

Interstitial fluorine doping TiO_2 photocatalysts were successfully prepared by gas–liquid plasma technology using NaF, NaF combined with $[C_4MIM]HSO_4$, and $[C_4MIM]BF_4$, as the fluorine precursors, respectively. Ionic liquids used in our work were beneficial to the formation of interstitial F-doped TiO_2 . The interstitial doping fluorine ions were thermally stable against calcination under the temperature of $500^\circ C$. And they showed mesoporous structure, better crystallinity and higher photocatalytic activity for MB degradation. Notably, the $F-[C_4MIM]BF_4-TiO_2$

sample showed the highest photocatalytic activity, which was 42 times higher than its photolysis and was about 2.9 times as that prepared without addition of ionic liquid. FTIR results indicate that $[C_4MIM]BF_4$ ionic liquid is stable under plasma treatment.

Acknowledgements This work is supported by National Natural Science Foundation of China (Grant Nos. 21673026, 11505019, 21173028), Dalian Youth Science and Technology Project (Grant No. 2015R089).

References

- Giannakas AE, Antonopoulou M, Daikopoulos C, Deligiannakis Y, Konstantinou I (2016) Appl Catal B 184:44
- Wu HB, Hng HH, Lou XW (2012) Adv Mater 24:2567
- Liu B, Aydil ES (2009) J Am Chem Soc 131:3985
- Wang DH, Choi D, Li J, Yang ZG, Nie Z, Kou R, Hu D, Wang CM, Saraf LV, Zhang J, Aksay IA, Liu J (2009) ACS Nano 3:907
- Wang CX, Yin LW, Zhang LY, Qi YX, Lun N, Liu NN (2010) Langmuir 26:12841
- Asahi R, Morikawa T, Ohwaki T, Aoki K, Taga Y (2001) Science 293:269
- He ZL, Que WX, Chen J, Yin XT, He YC, Ren JB (2012) ACS Appl Mater Interfaces 4:6816
- Yu JG, Li Q, Liu SW, Jaroniec M (2013) Chem Eur J 19:2433
- Xiang QJ, Yu JG, Jaroniec M (2011) Phys Chem Chem Phys 13:4853
- Yu W, Liu XJ, Pan LK, Li JL, Liu JY, Zhang J, Li P, Chen C, Sun Z (2014) Appl Surf Sci 319:107
- Pan JH, Cai ZY, Yua Y, Zhao XS (2011) J Mater Chem 21:11430
- Hsieh K, Wang HJ, Locke BR (2016) J Hazard Mater 317:188
- Yu M, Zhai LY, Zhou Q, Li CP, Zhang XL (2012) Appl Catal A 419:53
- Hatakeyama Y, Kimura S, Kameyama T, Agawa Y, Tanaka H, Judai K, Torimoto T, Nishikawa K (2016) Chem Phys Lett 658:188
- Tran QC, Dao VD, Jung KD, Choi HS (2014) Electrochim Acta 143:357
- Zhou T, Jang K, Jang BWL (2013) Catal Today 211:147
- Zhang XL, Di LB, Zhou Q (2013) J Energy Chem 22:446
- Wei ZH, Liu CJ (2011) Mater Lett 65:353
- Zhang XL, Zhang LJ, Li YC, Di LB (2015) Catal Today 256:215
- Zhan ZB, Di LB, Zhang XL, Li YC (2016) Plasma Sci Technol 5:494
- Di LB, Xu ZJ, Wang K, Zhang XL (2013) Catal Today 211:109
- Huang GL, Zhu YF (2007) J Phys Chem C 111:11952
- Huang GL, Zhang SC, Xu TG, Zhu YF (2008) Environ Sci Technol 42:8516
- Pan JH, Zhang XW, Du AJ, Sun DD, Leckie JO O (2008) J Am Chem Soc 130:11256
- Yu JC, Yu JG, Ho WK, Jiang ZT, Zhang LZ (2012) Chem Mater 14:3808
- Zhou JK, Lv L, Yu JQ, Li HL, Guo PZ, Sun H, Zhao XS (2008) J Phys Chem 112:5316
- Yua CL, Fan QZ, Xie Y, Shu Q, Yu JC (2012) J Hazard Mater 237–238:38
- Fu HB, Zhang SC, Xu TG, Zhu YF, Chen JM (2008) Environ Sci Technol 42:2085